eNeuro

Research Article: New Research | Sensory and Motor Systems

Disruption of hyaluronic acid in skeletal muscle induces decreased voluntary activity via chemosensitive muscle afferent sensitization in male mice

https://doi.org/10.1523/ENEURO.0522-21.2022

Cite as: eNeuro 2022; 10.1523/ENEURO.0522-21.2022

Received: 16 November 2021
Revised: 25 February 2022
Accepted: 9 March 2022

Title: Disruption of hyaluronic acid in skeletal muscle induces decreased voluntary activity via chemosensitive muscle afferent sensitization in male mice.

Abbreviated Title: Muscle HA disruption sensitizes chemoreceptors

Luis F Queme[1,2,5], Adam Dourson[1], Megan C Hofmann[1], Ally Butterfield[1], Rudolph D. Paladini[3*], Michael P Jankowski[1,2,4,5]

1. **Department of Anesthesia, Division of Pain Management, Cincinnati Children's Hospital Medical Center, Cincinnati, OH 45229**
2. **Department of Anesthesiology, University of Cincinnati, Cincinnati, OH 45229**
3. **Halozyme, Inc. San Diego, CA 92121**
4. **Department of Pediatrics, University of Cincinnati College of Medicine, Cincinnati, OH 45229.**
5. **Pediatric Pain Research Center, Cincinnati Children's Hospital Medical Center, Cincinnati, OH 45229**

***Current Institution: Halo Biosciences, Stanford, CA 94301**

Author Contributions: LFQ, AD, AB, and MCH Performed Research. LFQ, RP, and MPJ Designed Research. LFQ, AD, and MPJ Wrote the paper.

Correspondence should be addressed to:
Michael P Jankowski
3333 Burnet Avenue, MLC6016
Cincinnati, Ohio 45229-3026
Telephone: (513) 803-7966
E-mail: michael.jankowski@cchmc.org

Number of Figures: 4
Number of Tables: 3
Number of words for Abstract: 250
Number of words for Significance Statement: 120
Number of words for Introduction: 593
Number of words for Discussion: 1673

Conflict of Interest: Yes. This research was performed while under a research contract with Halozyme Inc., manufacturers of the hyaluronidase product used (PEGPH20).

Funding sources: This work was partially funded by a research contract with Halozyme Inc. This work was also supported by a grant to MPJ from the NIH (R01NS113965).

Abstract:

PEGPH20, a human recombinant hyaluronidase, has been proposed as a coadjutant to pancreatic cancer chemotherapy. In early trials, patients reported increased widespread muscle pain as the main adverse reaction to PEGPH20. To understand how PEGPH20 caused musculoskeletal pain, we systemically administered PEGPH20 to male mice and measured voluntary wheel activity and pain-related behaviors. These were paired with ex-vivo electrophysiology of primary sensory neurons, whole DRG realtime PCR, and immunohistochemistry of hindpaw muscle. PEGPH20 induced significantly lower wheel running, compared to vehicle treated animals, and decreased mechanical withdrawal thresholds 5 days after PEGPH20 injections. Chemo-sensory muscle afferents showed increased responses to noxious chemical stimulation of their receptive fields in the PEGPH20 treated group. This was correlated with upregulation of the NGF receptor TrkA, the transient receptor potential vanilloid type 1 (TRPV1) channel and ATP-sensitive channel P2X3 in the DRG. Immunohistochemistry of hindpaw muscles revealed damage to the muscle architecture and extensive infiltration of the tissue by cells of the myelomonocytic lineage 3 days after PEGPH20 injection. Peripheral macrophage ablation in macrophage Fas-induced apoptosis (MaFIA) mice, however, did not prevent the decreased voluntary activity and instead caused even lower levels of running. These results suggest that disruption of hyaluronic acid within the muscle extracellular matrix sensitizes chemo-nociceptive muscle afferents possibly leading to altered pain-like behaviors. Ablation experiments suggest macrophages are necessary for adequate recovery of voluntary activity after hyaluronic acid (HA) disruption. These data support a role for HA and macrophages in tissue integrity and muscle pain development in patients taking PEGPH20.

Significance Statement:

Hyaluronidase co-administration has been suggested as a possible solution to improve the delivery of chemotherapeutic agents into difficult to access tissues. In clinical trials, patients receiving a systemic dose of hyaluronidase reported widespread pain as a side effect. Delivering hyaluronidase to mice, we found that they experienced decreased voluntary activity. We observed alterations in the response properties of metabo-nociceptive muscle afferents, accompanied by increased muscle infiltration of myeloid lineage cells including macrophages. Macrophage depletion at the time of hyaluronidase administration surprisingly exacerbated the decrease in voluntary activity. This suggests that increased hyaluronidase levels can affect muscle function and lead to immune responses, but also suggest these cells may be needed for muscle recovery to allow animals to perform activity-based tasks.

Introduction:

Pain is a frequent, undesired effect of pharmacotherapies aimed at treating different conditions. In the case of therapeutics used for cancer, long lasting pain is a major problem. Recent studies have explored the use of a novel approaches to cancer therapeutics, such as the disruption of the tumoral stroma. One of the suggested approaches to achieve disruption of the tumor microenvironment includes the use of a pegylated recombinant human hyaluronidase (PEGPH20) to target hyaluronic acid (HA), a major component of the tumoral extracellular matrix. Initial, phase Ib trials exploring the use of this strategy in patients with pancreatic cancer, however, reported musculoskeletal pain as well as extremity pain accompanied by edema and fatigue as the most common PEGPH20-related adverse events (Hingorani et al., 2016). At sufficient doses (1mg/Kg), PEGPH20 increased the entry of therapeutic antibodies into the tumor

stroma (Manuel et al., 2015; Singha et al., 2015; Li et al., 2018). Thus, it is important to characterize the mechanism behind the observed side effects in order to maximize the potential benefits of this approach.

Hyaluronic acid is an important component of the extracellular matrix (ECM) within the skeletal muscles. It has been localized to the epimysium, perimysium, and endomysium (Laurent et al., 1991; Piehl-Aulin et al., 1991). It has also been associated with the perivascular and perineural connective tissue (Laurent et al., 1991; Piehl-Aulin et al., 1991). In contrast, smooth muscle seems almost devoid of HA (Laurent et al., 1991). As such, HA plays an important role in maintaining the healthy architecture of skeletal muscle. A previous report has shown that HA can be pro- or anti- nociceptive when injected in the skin, depending on its molecular weight (Ferrari et al., 2016). Low molecular weight HA, a subproduct of hyaluronidase activation and subsequent degradation of ECM HA during injury and inflammation, seems to be pronociceptive (Ferrari et al., 2016; Ferrari et al., 2018). Contrary to this, high molecular weight HA can be antinociceptive and ameliorate inflammatory pain (Ferrari et al., 2018; Bonet et al., 2020). Regardless of their opposing functions, both forms seem to be related to activation of the CD44 receptor in sensory neurons.

In contrast with the adverse effects reported in cancer patients, hyaluronidase has been used as a therapeutic agent to treat upper limb muscle stiffness in individuals with cerebral injury (Raghavan et al., 2016), without clinically significant side effects. The potential therapeutic benefit has also been reported in patients with myofascial pain syndrome (Ghasemi et al., 2020). These reports showing results in opposition to the adverse effects observed in larger clinical

trials in cancer patients, highlight the need to better understand the effects of systemic administration of hyaluronidases in the skeletal muscles and the mechanisms behind its effects on musculoskeletal pain.

In order to develop strategies to ameliorate the pain-related adverse effects of the administration of hyaluronidase, we explored the effects of systemic PEGPH20 administration in mice. Our working hypothesis was that intraperitoneal (i.p.) administration of PEGPH20 will induce widespread muscle pain potentially due to disruption of the normal muscle architecture that affects the sensory processing. To test this, we used a wheel running activity assay, along with evoked withdrawal to muscle squeezing, and grip strength, known methods to evaluate painful responses from the muscles in mice (Tappe-Theodor et al., 2019; Contreras et al., 2021) to examine the effects of PEGPH20 administration. We verified the effects of PEGPH20 on muscle architecture via immunohistochemical staining of the hindpaw muscles and evaluated potential changes in afferent function using a muscle-nerve-dorsal root ganglia-spinal cord *ex-vivo* preparation and realtime PCR on affected DRGs.

Methods:

Animals

Experiments were conducted with young adult male mice (3–8 wks) of the following backgrounds: C57BL/6J (C57), B6.129P2-Lyz2$^{tm1(cre)Ifo}$/J (LysMcre), B6.Cg-Gt(ROSA)26Sor$^{tm14(CAG-tdTomato)Hze}$/J (tdTom), C57BL/6-Tg(Csf1r-EGFP-NGFR/FKBP1A/TNFRSF6)2Bck/J also known as macrophage fas-induced apoptosis (MaFIA) mice (The Jackson Laboratory, Bar Harbor, ME) and littermate controls. All animals were

housed in a barrier facility in group cages of no more than 4 mice, maintained on a 12:12-h light-dark cycle with a temperature-controlled environment, and given food and water ad-libitum. All procedures were approved by the [Author Institution] Institutional Animal Care and Use Committee and adhered to NIH Standards of Animal Care and Use under AAALAC approved practices.

Administration of PEGPH20 and AP compound

A single dose of PEGPH20 or its vehicle solution (10nM Histidine, 130nM NaCl, pH 6.5) (provided by Halozyme, Inc.) was administered at a dose of 1mg/kg i.p.; the same effective dose used in clinical trials (Li et al., 2018). The designer drug AP20187 (AP) was administered to the MaFIA mice i.p. for seven days at a dose of 10 mg/kg for experiments utilizing these animals.

Evoked pain-related behaviors

Testing of pain-related behaviors, withdrawal thresholds to muscle squeezing and grip strength, have been performed previously (Ross et al., 2014; Queme et al., 2016; Queme et al., 2020). Mice were first tested at baseline, as well as 1, 3, 5, and 7 days after the administration of either PEGPH20 or vehicle, which were administered immediately after the baseline measurements.

Mechanical withdrawal thresholds were determined by squeezing the hindpaw muscle with a modified Paw Pressure Meter (World Precision Instruments, Sarasota, FL), fitted with a rounded blunt probe that applied pressure to the plantar surface in order to stimulate deeper tissues. The withdrawal threshold was recorded for 3 trials with 5-minute intervals between stimulations, and the average was used for analysis. Muscle strength was tested via a grip strength meter (BioSeb,

Vitrolles, France). Animals were held by the tail over a metal bar while support was provided for the forepaws in order to measure grip strength exclusively on the hindpaw. Once the animal firmly held the bar with its hind paws, they were quickly pulled back horizontally (along the axis of the force sensor) until they could not retain their grip. Grip strength was measured (in g) in 3 rounds of 3 trials each, with 5 minutes between each round. The average of the nine trials was used for analysis.

Wheel running protocol

Animals were transferred from home cages to new cages fixed with a voluntary wheel attachment (Lafayette Instruments). Animals were singly housed with free access to food and water. The animals used in these experiments were used solely for the acquisition of voluntary wheel running behaviors and were not used for any measurements of pain-like behaviors or tissue analyses as previous literature (Grace et al., 2016; Ross et al., 2018) suggests a large role for voluntary wheel running on pain-like responses. For that same reason, voluntary activity was only monitored immediately after the administration of the PEGPH20 or vehicle, in an attempt to get a clear picture of the effects of the compound without the confounder of previous exercise. Either C57Bl/6 wildtype (WT) or MaFIA animals where used for these experiments. In groups treated with AP, seven daily IP injections (10 mg/kg) were administered 3 days prior to entry into the wheel cage and up to 4 days following entry. For all animals, PEGPH20 or vehicle was injected immediately before transfer to the wheel cages. Animals were housed in the wheel cages for seven days. Measurements obtained from voluntary running included numbers of revolutions, mean velocity (m/min) and distance travelled obtained in hourly bins.

186 ***Ex vivo* recording preparation**

187 *Ex vivo* recording was performed as previously described (Dourson et al., 2021). Briefly, mice
188 were anesthetized with an intramuscular hindlimb injection of ketamine and xylazine (90 and 10
189 mg/kg, respectively) into the left leg and perfused transcardially with ice-chilled, oxygenated
190 (95% O2-5% CO2) artificial cerebrospinal fluid (aCSF; in mM: 127.0 NaCl, 1.9 KCl, 1.2
191 KH2PO4, 1.3 MgSO4, 2.4 CaCl2, 26.0 NaHCO3, and 10.0 D-glucose). The right hindpaw and
192 the spinal cord (SC) were then excised and placed in a bath of the same aCSF. The skin was
193 removed along with the cutaneous branches of all the nerves. The SC was hemisected and the
194 tibial nerve along with the distal hindlimb muscles innervated by this nerve (with bone left
195 intact), were dissected in continuity with their respective DRGs (L5, L4 and L3). After
196 dissection, the preparation was transferred to a separate recording chamber containing cold
197 oxygenated aCSF. The paw was pinned on an elevated platform, keeping the entire paw perfused
198 in a chamber isolated from the DRGs and the SC. Finally, the bath was slowly warmed to 32°C
199 before recording from the DRGs.
200
201 All single unit recordings were made from the L3 and L4 DRGs. Sensory neuron somata were
202 impaled with quartz microelectrodes (impedance>150MΩ) containing 5% Neurobiotin (Vector
203 Laboratories, Burlingame, CA) in 1M potassium acetate. Electrical search stimuli were delivered
204 through a suction electrode on the tibial nerve to locate sensory neurons with axons in this nerve.
205 The latency from the onset of this stimulus and the conduction distance between the DRG and
206 the stimulation site (measured directly along the nerve), were used to calculate the conduction
207 velocity (CV) of the fibers. Group IV afferents were classified as those with a CV≤ 1.2 m/s, and
208 group III afferents were those with CVs between 1.2 and 15 m/s. Peripheral receptive fields

(RFs) in the muscles were localized by electrically stimulating the muscles with a concentric bipolar electrode. Only driven cells with RFs in the muscles then underwent mechanical, thermal, and chemical testing. Mechanical response characteristics were assessed with an increasing series of von Frey hairs ranging from 0.4 g to 10 g (with diameters of 0.23–0.36 mm). Mechanical stimulation of the RF was held for approximately 1-2 seconds. Thermal responses were determined by applying hot (≥50°C) or cold (≤3°C) saline directly to the paw muscles at the electrically determined RF. Each application lasted ~1-2s. After that, the muscles were exposed to an oxygenated "low" metabolite mixture (15 mM lactate, 1 μM ATP, pH 7.0) and then to a "high" metabolite mixture (50 mM lactate, 5 μM ATP, pH 6.6) (Jankowski et al 2013) (Queme et al 2020). delivered by a valve controller with an in-line heater to maintain solutions at bath temperature. ATP was added to the mixture immediately prior to delivery of metabolites. Adequate recovery times (~20–30 s) were employed between stimulations. All elicited responses were recorded digitally for off-line analysis (Spike2 software, Cambridge Electronic Design). Because exposure to metabolites can alter the response properties of sensory neurons, all mechanical and thermal stimuli were repeated after exposure to metabolites. To verify that the quality of the recordings does not deteriorate though the duration of the experiment, responses from afferents recorded at the beginning and end of the experiment were grouped within conditions and compared. We did not detect significant differences between recorded units recorded at the beginning vs the end of the experiment.

Immunohistochemistry

In order to evaluate the integrity of the extracellular matrix and skeletal muscle fibers, we injected mice with 200uL of Evans-blue dye (i.p., 1% in 0.9% sterile saline solution)

immediately before administration of PEGPH20. Evans-blue Dye has been used extensively to evaluate the integrity and permeability of the membrane of muscle fibers (Hamer et al., 2002). Wheat germ agglutinin (WGA) conjugated with FITC (Life Technologies, Eugene, OR) was used to co-stain the tissue to visualize the membranes in the skeletal muscle, as previously described (Kostrominova, 2011). Briefly, muscle tissue was embedded in Tissue-Tek O.C.T. compound (Sakura Finetek USA Inc., Torrance, CA), flash frozen in liquid nitrogen and sectioned at 10μM on a cryostat and mounted on slides. Tissue was fixed on slide using 4% PFA in 0.1 M phosphate buffered saline (PBS). The samples were subsequently washed, blocked in 0.01M PBS containing 5% horse serum, 1% bovine serum albumin and 0.2% TritonX-100 for 10 min. Sections were stained with WGA-FITC (1:100), incubated for an hour, washed and cover slipped. A separate set of muscle samples from mice expressing a florescent reporter (tdTomato) on cells of myelomonocytic lineage (macrophages) were co-stained with Dystrophin (rabbit anti-dystrophin 1:250; Abcam, cat. No. ab15277), incubated overnight and labeled with secondary antibodies (AlexaFluor 488, 1:400; Jackson immunoresearch Laboratories, West Grove, PA) and cover slipped. Exposure time during microscopic analysis for each image was performed at the same intensity level to confirm staining above background. Distribution of fluorescent staining was determined with a Nikon confocal microscope with sequential scanning to avoid bleed-through of the fluorophores. Images were captured at 40X magnification. 3 nonconsecutive sections, separated at least by 4 sections, from 3 different animals per condition were used to quantify the percentage of myofibers positive for EBD. All the muscle cells in a section were labeled using image J and muscle cells that were observed to contain red staining were considered positive. The percentage of positive cells obtained from each animal was used for comparisons. Similar methods were used to quantify LysM;tdTom cells in the muscle.

Macrophage ablation after AP compound administration was confirmed via confocal imaging of the full hindpaw of the mouse. As before, 3 nonconsecutive sections from 3 different animals per condition were used to quantify the area covered by GFP signal via ImageJ software. Minimum intensity threshold was set at 60 and maximum at 255. Average intensity per animal was determined among the 3 sections and data was then averaged across animals per group for comparisons. Images for publication were prepared using Photoshop Elements software (Adobe, San Jose, CA, USA).

RNA Isolation and Realtime PCR

DRG (L3-L4, right side) tissue was collected from PEGPH20, or vehicle treated conditions at different time points. Tissue RNA was isolated using the Qiagen RNeasy kit, according to the manufacturer's protocol. Fort realtime PCR, 500ng of total RNA was DNAse I treated (Invitrogen) and reverse transcribed using Superscript II (Invitrogen) reverse transcriptase. 20ng of cDNA were used in SYBR Green realtime PCR reactions that were performed in duplicate and analyzed on a Step-One realtime PCR machine (Applied Biosystems).

Primer sequences for GAPDH, ASIC3, TRPV1, TRPA1, TrkA, GFRα3 were obtained from Elitt et al. (Elitt et al., 2006). Primer sequences used for GFRα1, GFRα2, and P2X3 were obtained from Jankowski et al. (Jankowski et al., 2009). Primer sequences for IL1r1 and P2X5 have been reported previously (Ross et al., 2014). Cycle time (Ct) values for all targets were all normalized to a GAPDH internal control. Ct values (used to determine fold change after injury) were then obtained by subtracting the normalized target gene's Ct value from naive controls. Then fold change was determined as $2^{\Delta\Delta Ct}$ (Applied Biosystems). The error of the difference in means is

then also calculated for the fold-change. Values were then converted and reported as a percent change where 2-fold change = 100% change.

Statistical analysis

All values are presented as mean ± SEM unless stated differently. Behavioral assays, RT qPCR data, and comparisons of electrophysiological responses were tested with a 1-way ANOVA, or a 2-way repeated measures (RM) ANOVA with Bonferroni's post hoc test when appropriate. Two group comparisons that failed normality tests were tested with a Mann-Whitney U-test. Percentage of EBD positive cells was compared using a Chi-square test. Critical significance level was set at $p<0.05$.

Statistics table

	Data Structure	Type of test	Comparison	95% Confidence interval
a	Normally distributed	Two-way RM ANOVA		
		Bonferroni post-hoc test	PEGPH20 vs API Buffer Day 1	368.4 to 7286
		Bonferroni post-hoc test	PEGPH20 vs API Buffer Day 2	67.36 to 6985
		Bonferroni post-hoc test	PEGPH20 vs API Buffer Day 3	695.6 to 7613
b	Normally	Two-way RM		

	distributed	ANOVA		
		Bonferroni post-hoc test	PEGPH20 vs Vehicle Day 5	11.85 to 146.1
c	Normally distributed	Two-way RM ANOVA	Bonferroni post-hoc test	-8.005 to 12.52
d	Non-normally distributed	Kruskal-Wallis test		Test does not generate confidence interval
e	Non-normally distributed	Mann Whitney U-test		-1.000 to 3.000
f	Non-normally distributed	Mann Whitney U-test		-1.000 to 2.000
g	Non-normally distributed	Mann Whitney U-test		-80.66 to 89.10
h	Non-normally distributed	Mann Whitney U-test		1.700 to 24.62
i	Non-normally distributed	Mann Whitney U-		-12.70 to 24.30

		test		
j	Non-normally distributed	Mann Whitney U-test		1.700 to 24.62
k	Normally distributed	Chi-square test		Test does not generate confidence interval
l	Normally distributed	Unpaired T-test		22155 to 108900
m	Normally distributed	Mixed-effects analysis	PEGPH20 vs Vehicle Day 1	-7169 to -963.0
		Bonferroni post-hoc test	PEGPH20 vs Vehicle Day 2	-6877 to -456.6
		Bonferroni post-hoc test	PEGPH20 vs Vehicle Day 3	-8772 to -279.7
		Bonferroni post-hoc test	PEGPH20 vs PEGPH20+AP Day4	110.9 to 2674
		Bonferroni post-hoc test	PEGPH20 vs PEGPH20+AP Day 5	309.0 to 2507
		Bonferroni	PEGPH20 vs	389.1 to 3866

		post-hoc test	PEGPH20+AP Day 6	
		Bonferroni post-hoc test	PEGPH20 vs PEGPH20+AP Day 7	580.0 to 3549
n	Normally distributed	One-way RM ANOVA		
		Bonferroni post-hoc test	PEGPH20 vs PEGPH20+AP	395.7 to 2221
		Bonferroni post-hoc test	PEGPH20 vs Vehicle	-4459 to -2177
		Bonferroni post-hoc test	PEGPH20+AP vs Vehicle	-5256 to -3997
		Bonferroni post-hoc test	AP vs Vehicle	1464 to 4666

Results:

PEGPH20 induces long lasting reductions in voluntary activity as well as increased pain-related behaviors.

Based on previous reports, we evaluated the effect of PEGPH20 on the activity levels of uninjured mice. To do this we administered PEGPH20 or vehicle solution at 1mg/kg i.p. The mice injected with vehicle ran approximately the same distance every day, preferentially during the night phase of the illumination cycle. Immediately after the administration of PEGPH20, the

297 mice showed significantly lower activity than their vehicle injected counterparts (Fig 1A[a]).
298 Activity remained significantly lower during the first 3 days after the administration of
299 PEGPH20 and did not recover to the same level of activity observed in vehicle treated animals
300 during the testing period.
301
302 In separate cohorts of mice, we tested pain related behaviors 1 day before the administration of
303 PEGPH20 or vehicle and continued testing 1 day after the administration and every other day up
304 to 7 days (Fig 1B[b]). We did not detect any changes in the mechanical withdrawal thresholds to
305 muscle squeezing at 1, and 3 days after compound administration. In contrast, 5 days after the
306 administration of PEGPH20 there was a significant decrease in the mechanical withdrawal
307 threshold. This decrease in withdrawal threshold reversed 7 days after PEGPH20 administration.
308 Finally, we tested grip strength in the hind paws. While the mean grip strength increased slowly
309 after day 1 (Fig 1C[c]), both groups followed the same pattern and there were not significant
310 differences between the group that received PEGPH20 or the group that received vehicle.
311
312 **PEGPH20 induces changes in the response properties of primary sensory neurons to a**
313 **noxious combination of metabolites.**
314 Using an *ex-vivo* muscle-nerve-DRG-spinal cord preparation, we performed single unit
315 recordings from afferents innervating the right hindpaw muscles at 1 and 3 days after the
316 administration of PEGPH20 or vehicle. Preliminary analysis did not reveal differences between
317 the recordings captured at 1 or 3 days for both groups as shown in Table 1[d], so both timepoints
318 were merged into one group for each condition. As shown in Fig 2A,B[e,f], we did not find any
319 significant differences in the afferent response properties to mechanical stimulation. No changes

in either threshold, instantaneous frequency (IF), or firing rate (FR) were observed between conditions. There were also no significant differences in the responses to heat or cold stimulation (Fig 2C, D[g,h]). However, when we stimulated the preparation with different concentrations of metabolites (lactate, ATP, and low pH) resembling the environment in the muscle during normal work-related activity (Low metabolites) or ischemic contractions (High metabolites), we found no differences in the response pattern to the low concentration of metabolites, but found an increased response of group III/IV afferents (IF) to higher concentrations of these metabolites in the group that was treated with PEGPH20 compared with vehicle treated controls (Fig 2E,F[i,j]).

PEGPH20 causes a breakdown of the membranes within the muscle as well as an increased infiltration by LysM-tdTom cells.

The target of PEGPH20 is hyaluronic acid (HA), an important structural component of the architecture of skeletal muscle. We suspected that the effects of PEGPH20 on voluntary activity and response properties of skeletal muscle afferents could be explained by changes in the structure of the muscle. As shown in Figure 3A,B[k], 1 day after the administration of PEGPH20, we observed widespread staining of the muscle tissue with Evans-blue dye, suggesting a disruption of the membranes within the skeletal muscles. In the mice treated with vehicle, there is very low Evans-blue leakage into the muscle.

Tissue injury has frequently been associated with increased infiltration of the affected tissue by immune cells. In particular, macrophages are known to play an important role not only in the development of muscle pain in other models but have also been suggested to play an important role in the subsequent repair of the injured tissue. In order to evaluate if macrophages could be

343 playing a role in the increased musculoskeletal pain secondary to PEGPH20 administration, we
344 administered PEGPH20 to mice expressing a fluorescent reporter protein in cells of
345 myelomonocytic lineage (LysMcre/TdTomato mice). 3 days after the administration of
346 PEGPH20, we observed widespread infiltration of myeloid lineage cells into skeletal muscle
347 (Fig. 3C) compared with little infiltration in the vehicle treated animals (Veh: 3.9±1.9 vs
348 PEGPH20: *32± 3.4; t=6.46, df=4; *p<0.003, t-test).
349
350 To better understand the effects of the alterations in the musculoskeletal structure in the changes
351 observed in response properties of primary muscle afferents, we isolated RNA from whole DRGs
352 (L3 and L4) and performed realtime PCR. We tested for a variety of genes at 1 day after
353 PEGPH20 administration. We did not observe significant changes in gene expression 1 day after
354 PEGPH20 administration. 3 days after injection of PEGPH20, however, we observed a
355 significant upregulation in the P2X receptor 3 (P2X3), and a decrease in the expression of the
356 GDNF receptor, GFRα1 and the Interleukin-1 receptor IL-1r1. By day 5 we observed a
357 significant decrease in the expression of the NGF receptor TrkA reverting the trend observed in
358 day 1 and day 3. No changes were observed at 7d with the exception of P2X3 which remained
359 elevated 7 days after injury (Table 2).
360
361 **Ablation of macrophages does not improve the effects of PEGPH20 on voluntary activity**
362 Our previous observation of infiltration by cells of myelomonocytic lineage in the skeletal
363 muscle after PEGPH20 administration suggested that these immune cells may be playing a
364 significant role in the development of long-lasting muscle pain. To test if macrophages played
365 any role in the development of decreased voluntary activity after PEGPH20 administration, we

366 decided to ablate them in mice with PEGPH20 injection and assayed voluntary running. To do
367 this, we used macrophage fas-induced apoptosis (MaFIA) mice. MaFIA mice are a transgenic
368 line that, when injected with the designer drug AP20187 (AP) temporarily ablates peripheral
369 macrophages and dendritic cells. Our injection protocol replicated the dose and scheme used in
370 previous studies that showed evident macrophage depletion 24h after the third injection (Burnett
371 et al., 2004). Other works using lower doses than our protocol report up to 90% depletion of
372 circulating monocytes that does not recuperate until 4 days after the last dose of AP (Yu et al.,
373 2020). We confirmed the effectiveness of this strategy via immunohistochemistry. MaFIA mice
374 treated with PEGPH20 + AP compound had significantly less GFP signal in the hindpaw
375 compared to PEGPH20 + Vehicle treated animals (Fig 4 A, B[l]). This approach insured that
376 macrophages were not present in the periphery at the time of PEGPH20 administration and that
377 the macrophage population would not start to recover until after at least 5 days into the running
378 experiment, allowing for the observation of the voluntary activity pattern of the mice when
379 exposed to hyaluronidase, but lacking peripheral macrophage infiltration.
380 We found that the injection of PEGPH20 reduced the distance that animals traveled in all groups
381 compared to vehicle controls and that ablation of macrophages by injection of AP did not
382 ameliorate the effects of PEGPH20. In fact, while animals injected with only PEGPH20 showed
383 a small recovery of the traveled distance at days 6 and 7, the animals that received AP in
384 combination with PEGPH20 did not show any recovery (Fig 4C[m]). Administration of AP alone
385 induced a significant decrease in activity compared to the vehicle treated mice and almost in line
386 with the decrease observed after administration of PEGPH20 (Table 3). This suggests that
387 macrophage depletion can have a big impact on mouse behavior and should always be
388 considered when using MaFIA mice as a model. When we compared the total running distance

of mice injected with PEGPH20 or AP alone to the combination of both PEGPH20 and AP, the combination group showed an additive effect, reducing voluntary activity almost completely. We found that animals injected with both compounds ran significantly less than those injected with either one compound alone, as well as from controls (Fig. 4C[m], D[n]). This suggests that the presence of macrophages in the skeletal muscle after the disruption of the architecture by hyaluronidase administration may be protective and may be more important for the recuperation of the mice from hyaluronidase treatment than for the development of the decreased voluntary activity.

Discussion:

Pharmacological therapies for cancer frequently result in the undesired adverse effect of pain (Fallon, 2013; Masocha, 2018). As the search for novel therapeutic approaches expands, it is logical to expect different clinical presentations. Recently, therapies involving the administration of hyaluronidase systemically as a potential enhancer of chemotherapeutic approaches for pancreatic cancer have been explored (Hingorani et al., 2016). One of the observed adverse effects of this approach was widespread muscle pain (Hingorani et al., 2016). In contrast, in other clinical settings, hyaluronidase has been used successfully in ophthalmic surgery as an enhancer of local anesthesia (Buhren et al., 2016; Rüschen et al., 2018). The potential of the enzyme to disrupt connective tissue adhesions has led to the off-label use of this enzyme for the treatment of epidural adhesions associated with chronic back pain (Dunn et al., 2010) or to treat myofascial pain syndrome secondary to tissue contractures (Raghavan et al., 2016; Ghasemi et al., 2020). Recent reports have explored the specific role of HA in the sensitization of primary sensory neurons. Several reports suggest that high-molecular-weight HA (HMWHA) can reduce

413 inflammation-induced hyperalgesia (Ferrari et al., 2018; Bonet et al., 2020), while its
414 counterpart, low-molecular-weight HA (LMWHA) is capable of inducing mechanical
415 hyperalgesia (Ferrari et al., 2016). Furthermore, it has been reported that digestion of HMWHA
416 by hyaluronidase produces LMWHA and that the later can inhibit the differentiation of
417 monocytes that infiltrate tissue after injury into fibrocytes, cells that help in the repair of tissue
418 after injury (Maharjan et al., 2011). These findings would be in line with our observations and
419 would explain why the administration of PEGPH20 not only increases the recruitment of
420 myeloid lineage cells such as macrophages into the affected muscle but would also explain why
421 the removal of cells of myelomonocytic lineage aggravates the effects of PEGPH20
422 administration.
423
424 In this study, we aimed to further characterize the effects of systemic administration of
425 PEGPH20 in the development of widespread pain and determine the contribution of muscle
426 primary sensory neurons in this phenomenon. In accordance with clinical observations, our mice
427 experienced an immediate decrease in voluntary wheel running after the administration of
428 PEGPH20. Voluntary wheel running has been shown to be a reliable pain assessment tool in
429 rodents (Ross et al., 2018; Kandasamy and Morgan, 2021) and has been shown to recuperate
430 faster than evoked measurements, closely replicating the recovery observed in the clinical setting
431 (Kandasamy et al., 2016). These differences between the results observed from voluntary
432 running and the evoked pain-related behaviors (muscle squeezing), can explain why we are able
433 to observe an acute drop in the activity, but we do not detect changes in withdrawal thresholds
434 until 5 days after injection. It is also relevant that in our behavioral assessments, we did not
435 observe a decrease in overall grip strength suggesting that the effects of PEGPH20 do not alter

436 the ability to forcefully contract muscles and that the differences in activity are more
437 representative of pain-like effects under these specific conditions.
438
439 The lack of changes in the mechanical withdrawal thresholds at 1 and 3 days after PEGPH20
440 administration correlates very well with the observations in our electrophysiological recordings
441 where we did not detect any differences in the response to mechanical stimulation between
442 groups. Nevertheless, a limitation of this study lies in the fact that we did not perform
443 electrophysiological studies at 5 days after PEGPH20 administration that would facilitate the
444 understanding of the evoked behavioral changes observed a this timepoint. However, it is
445 interesting that we detected a significant difference in the responses to stimulation with high
446 metabolites, a combination of low pH, ATP and lactic acid that closely resembles the
447 environment in the muscle during painful, ischemic muscle contractions (Light et al., 2008;
448 Jankowski et al., 2009; Pollak et al., 2014; Ross et al., 2014; Queme et al., 2020). If this
449 specific subset of afferents, thought to perform the function of metabo-nociceptors is sensitized,
450 it is logical to expect that during intense muscle activity, the mice would experience increased
451 pain and thus avoid voluntary exercise. Since the changes in activity were so robust and were
452 detected very early on, it is likely that sensitization of these afferents is a larger driving force of
453 HA induced pain in humans rather than changes in mechanical nociceptors. It is important to
454 note that heat responsiveness in afferents is slightly, but not statistically increased after
455 PEGPH20 treatment. A future study assessing greater numbers of heat sensitive afferent would
456 be necessary however to determine this. Another important limitation of this study is that it was
457 only performed in male mice. Several conditions presenting with chronic musculoskeletal pain,

458 such as fibromyalgia, have a higher prevalence in females. It will therefore be important to
459 perform these studies in females to assess sex differences in responses to PEGPH20.
460
461 Multiple receptors have frequently been associated with the development of musculoskeletal
462 pain. Some of the receptors that have been traditionally associated with increased pain include
463 the NGF receptor TrkA (Hayashi et al., 2011; Queme et al., 2013; Oga et al., 2020) as well as the
464 ion channel TRPV1. Contrary to our expectations, neither of these receptors showed increased
465 expression after the administration of PEGPH20. In fact, TrkA it was significantly
466 downregulated 5 days after the administration of hyaluronidase. While these results are
467 indicative of directionality, it is worth noting that further experimentation is needed to
468 understand if the mRNA expression profile observed after administration of PEGPH20 is also
469 translated to protein levels (Schindler et al., 1990; Raqib et al., 1996; Donlin-Asp et al., 2021)
470 Other receptors that have been frequently associated with the development of muscle pain in the
471 context of ischemia, such as the interleukin 1 receptor, IL-1r1(Ross et al., 2016), and the GDNF
472 receptor GFRα1 (Queme et al., 2020) were also found to be downregulated at several timepoints
473 after the administration of PEGPH20. Previous studies have shown that ischemic injury of the
474 muscle can induce upregulation of these receptors. It is plausible that direct injury of the muscle
475 cells is necessary to cause this upregulation and that disruption of the extracellular matrix is
476 causing sensitization of primary muscle afferents via a completely different mechanism. In
477 contrast, the P2X3 receptor is known to be upregulated in the DRG after ischemic muscle
478 injuries (Ross et al., 2014; Ross et al., 2016), and has been linked to inflammatory pain
479 development (Queme et al., 2017). This receptor may therefore play a role in the development of
480 pain and decreased voluntary activity in these experiments. As an ATP sensitive ion channel,

increased expression of P2X3 could be involved in the increased responses observed in the chemo-nociceptive muscle afferents.

The increased presence of myelomonocytic-lineage cells in the muscle tissue after PEGPH20 administration suggested an important role for these immune cells. We hypothesized that macrophage infiltration in the muscle may be playing a role in sensitizing primary muscle afferents as this has been shown in different models of musculoskeletal pain (Gong et al., 2016; Oliveira-Fusaro et al., 2020). We tested this by ablating the peripheral macrophage population during PEGPH20 administration. Contrary to our predictions, we did not observe a recuperation of the voluntary activity when we administered PEGPH20 in combination with AP. In fact, we observed a marked decrease in the total activity of the animals. Previous work has shown that after systemic depletion of macrophages, nerve injury related pain can be prevented (Yu et al., 2020). However, in that study, depletion of the macrophages infiltrating the DRG after nerve injury was required to prevent the development of pain. A recent study used a tourniquet-based model of complex regional pain syndrome (CRPS), to induce musculoskeletal pain and showed that depletion of macrophages could prevent the development of pain after ischemic injury (De Logu et al., 2020). These studies, show that macrophages are necessary for the development of musculoskeletal pain. In contrast with our observations, neither of the models used in the previous work, result in the disruption of the ECM and the potential generation of LMWHA that would be expected after the administration of hyaluronidase.

Other studies using the MaFIA mouse line have reported that AP compound administration can induce malaise, intra-abdominal tissue adhesion and weight loss in mice (Burnett et al., 2004; Yu

et al., 2020). Interestingly, we found that AP alone induced a significant decrease in the overall activity levels comparable to the effect of PEGPH20 alone. A previous study using the MaFIA mouse line found that systemic administration of AP could cause significant weight loss and increased baseline mechanical thresholds (Yu et al., 2020). In the current study, we observed an additive effect in MaFIA animals treated with AP and PEGPH20, where animals had overall lower activity than either group alone. These data and the previous work indicate that the removal of myeloid-lineage cells results in both acute mechanical alterations, as well as prolonged prevention of physical activity. However, future studies using these animals should consider assessing multiple parameters as weight, mechanical thresholds, and activity are all affected by monocyte/macrophage ablation.

Macrophages are also known to play an important role in tissue repair after injury (Wynn and Vannella, 2016). They play an important role in the initiation maintenance and resolution phases of tissue repair (Mantovani et al., 2013; Wynn and Vannella, 2016; Kim and Nair, 2019). As such, it is possible that instead of preventing the development of muscle pain, macrophage ablation prevented the resolution of pain after PEGPH20 administration. This result is an important consideration for future therapies that desire to target macrophage depletion for pain relief.

Overall, this study highlights how systemic administration of hyaluronidase can disrupt the architecture of skeletal muscle, inducing sensitization of primary muscle afferents and leading to pain-like behaviors. Under these conditions, macrophages may be playing an important role in the resolution of injury instead of driving the initiation of pain. Our results also point out at the

possibility that macrophages are needed to resolve damage to skeletal muscle and potential therapies should not focus exclusively in removing or inhibiting macrophages but consider the possibility of harnessing their injury resolving properties as potential therapeutic options.

References:

Bonet IJM, Araldi D, Khomula EV, Bogen O, Green PG, Levine JD (2020) Mechanisms Mediating High-Molecular-Weight Hyaluronan-Induced Antihyperalgesia. J Neurosci 40:6477-6488.

Buhren BA, Schrumpf H, Hoff NP, Bölke E, Hilton S, Gerber PA (2016) Hyaluronidase: from clinical applications to molecular and cellular mechanisms. Eur J Med Res 21:5.

Burnett SH, Kershen EJ, Zhang J, Zeng L, Straley SC, Kaplan AM, Cohen DA (2004) Conditional macrophage ablation in transgenic mice expressing a Fas-based suicide gene. J Leukoc Biol 75:612-623.

Contreras KM, Caillaud M, Neddenriep B, Bagdas D, Roberts JL, Ulker E, White AB, Aboulhosn R, Toma W, Khalefa T, Adel A, Mann JA, Damaj MI (2021) Deficit in voluntary wheel running in chronic inflammatory and neuropathic pain models in mice: Impact of sex and genotype. Behav Brain Res 399:113009.

De Logu F, De Prá SD, de David Antoniazzi CT, Kudsi SQ, Ferro PR, Landini L, Rigo FK, de Bem Silveira G, Silveira PCL, Oliveira SM, Marini M, Mattei G, Ferreira J, Geppetti P, Nassini R, Trevisan G (2020) Macrophages and Schwann cell TRPA1 mediate chronic allodynia in a mouse model of complex regional pain syndrome type I. Brain Behav Immun 88:535-546.

Donlin-Asp PG, Polisseni C, Klimek R, Heckel A, Schuman EM (2021) Differential regulation of local mRNA dynamics and translation following long-term potentiation and depression. Proceedings of the National Academy of Sciences 118:e2017578118.

Dourson AJ, Ford ZK, Green KJ, McCrossan CE, Hofmann MC, Hudgins RC, Jankowski MP (2021) Early Life Nociception is Influenced by Peripheral Growth Hormone Signaling. J Neurosci 41:4410-4427.

Dunn AL, Heavner JE, Racz G, Day M (2010) Hyaluronidase: a review of approved formulations, indications and off-label use in chronic pain management. Expert Opin Biol Ther 10:127-131.

Elitt CM, McIlwrath SL, Lawson JJ, Malin SA, Molliver DC, Cornuet PK, Koerber HR, Davis BM, Albers KM (2006) Artemin overexpression in skin enhances expression of TRPV1 and TRPA1 in cutaneous sensory neurons and leads to behavioral sensitivity to heat and cold. J Neurosci 26:8578-8587.

Fallon MT (2013) Neuropathic pain in cancer. Br J Anaesth 111:105-111.

Ferrari LF, Araldi D, Bogen O, Levine JD (2016) Extracellular matrix hyaluronan signals via its CD44 receptor in the increased responsiveness to mechanical stimulation. Neuroscience 324:390-398.

Ferrari LF, Khomula EV, Araldi D, Levine JD (2018) CD44 Signaling Mediates High Molecular Weight Hyaluronan-Induced Antihyperalgesia. The Journal of neuroscience : the official journal of the Society for Neuroscience 38:308-321.

Ghasemi M, Mosaffa F, Hoseini B, Behnaz F (2020) Comparison of the Effect of Bicarbonate, Hyaluronidase, and Lidocaine Injection on Myofascial Pain Syndrome. Anesth Pain Med 10:e101037.

Gong WY, Abdelhamid RE, Carvalho CS, Sluka KA (2016) Resident Macrophages in Muscle Contribute to Development of Hyperalgesia in a Mouse Model of Noninflammatory Muscle Pain. J Pain 17:1081-1094.

Grace PM, Fabisiak TJ, Green-Fulgham SM, Anderson ND, Strand KA, Kwilasz AJ, Galer EL, Walker FR, Greenwood BN, Maier SF, Fleshner M, Watkins LR (2016) Prior voluntary wheel running attenuates neuropathic pain. Pain 157:2012-2023.

Hamer PW, McGeachie JM, Davies MJ, Grounds MD (2002) Evans Blue Dye as an in vivo marker of myofibre damage: optimising parameters for detecting initial myofibre membrane permeability. J Anat 200:69-79.

Hayashi K, Ozaki N, Kawakita K, Itoh K, Mizumura K, Furukawa K, Yasui M, Hori K, Yi SQ, Yamaguchi T, Sugiura Y (2011) Involvement of NGF in the rat model of persistent muscle pain associated with taut band. J Pain 12:1059-1068.

578 Hingorani SR, Harris WP, Beck JT, Berdov BA, Wagner SA, Pshevlotsky EM, Tjulandin SA, Gladkov OA,
579 Holcombe RF, Korn R, Raghunand N, Dychter S, Jiang P, Shepard HM, Devoe CE (2016) Phase Ib
580 Study of PEGylated Recombinant Human Hyaluronidase and Gemcitabine in Patients with
581 Advanced Pancreatic Cancer. Clin Cancer Res 22:2848-2854.
582 Jankowski MP, Rau KK, Ekmann KM, Anderson CE, Koerber HR (2013) Comprehensive phenotyping of
583 group III and IV muscle afferents in mouse. J Neurophysiol 109:2374-2381.
584 Jankowski MP, Lawson JJ, McIlwrath SL, Rau KK, Anderson CE, Albers KM, Koerber HR (2009)
585 Sensitization of cutaneous nociceptors after nerve transection and regeneration: possible role of
586 target-derived neurotrophic factor signaling. J Neurosci 29:1636-1647.
587 Kandasamy R, Morgan MM (2021) 'Reinventing the wheel' to advance the development of pain
588 therapeutics. Behav Pharmacol 32:142-152.
589 Kandasamy R, Calsbeek JJ, Morgan MM (2016) Home cage wheel running is an objective and clinically
590 relevant method to assess inflammatory pain in male and female rats. J Neurosci Methods
591 263:115-122.
592 Kim SY, Nair MG (2019) Macrophages in wound healing: activation and plasticity. Immunol Cell Biol
593 97:258-267.
594 Kostrominova TY (2011) Application of WGA lectin staining for visualization of the connective tissue in
595 skeletal muscle, bone, and ligament/tendon studies. Microsc Res Tech 74:18-22.
596 Laurent C, Johnson-Wells G, Hellström S, Engström-Laurent A, Wells AF (1991) Localization of
597 hyaluronan in various muscular tissues. A morphological study in the rat. Cell Tissue Res
598 263:201-205.
599 Li X, Shepard HM, Cowell JA, Zhao C, Osgood RJ, Rosengren S, Blouw B, Garrovillo SA, Pagel MD,
600 Whatcott CJ, Han H, Von Hoff DD, Taverna DM, LaBarre MJ, Maneval DC, Thompson CB (2018)
601 Parallel Accumulation of Tumor Hyaluronan, Collagen, and Other Drivers of Tumor Progression.
602 Clin Cancer Res 24:4798-4807.
603 Light AR, Hughen RW, Zhang J, Rainier J, Liu Z, Lee J (2008) Dorsal root ganglion neurons innervating
604 skeletal muscle respond to physiological combinations of protons, ATP, and lactate mediated by
605 ASIC, P2X, and TRPV1. J Neurophysiol 100:1184-1201.
606 Maharjan AS, Pilling D, Gomer RH (2011) High and low molecular weight hyaluronic acid differentially
607 regulate human fibrocyte differentiation. PLoS One 6:e26078.
608 Mantovani A, Biswas SK, Galdiero MR, Sica A, Locati M (2013) Macrophage plasticity and polarization in
609 tissue repair and remodelling. J Pathol 229:176-185.
610 Manuel ER, Chen J, D'Apuzzo M, Lampa MG, Kaltcheva TI, Thompson CB, Ludwig T, Chung V, Diamond DJ
611 (2015) Salmonella-Based Therapy Targeting Indoleamine 2,3-Dioxygenase Coupled with
612 Enzymatic Depletion of Tumor Hyaluronan Induces Complete Regression of Aggressive
613 Pancreatic Tumors. Cancer Immunol Res 3:1096-1107.
614 Masocha W (2018) Targeting the Endocannabinoid System for Prevention or Treatment of
615 Chemotherapy-Induced Neuropathic Pain: Studies in Animal Models. Pain Res Manag
616 2018:5234943.
617 Oga S, Goto K, Sakamoto J, Honda Y, Sasaki R, Ishikawa K, Kataoka H, Nakano J, Origuchi T, Okita M
618 (2020) Mechanisms underlying immobilization-induced muscle pain in rats. Muscle Nerve
619 61:662-670.
620 Oliveira-Fusaro MC, Gregory NS, Kolker SJ, Rasmussen L, Allen LH, Sluka KA (2020) P2X4 Receptors on
621 Muscle Macrophages Are Required for Development of Hyperalgesia in an Animal Model of
622 Activity-Induced Muscle Pain. Mol Neurobiol 57:1917-1929.
623 Piehl-Aulin K, Laurent C, Engström-Laurent A, Hellström S, Henriksson J (1991) Hyaluronan in human
624 skeletal muscle of lower extremity: concentration, distribution, and effect of exercise. J Appl
625 Physiol (1985) 71:2493-2498.

626 Pollak KA, Swenson JD, Vanhaitsma TA, Hughen RW, Jo D, White AT, Light KC, Schweinhardt P, Amann
627 M, Light AR (2014) Exogenously applied muscle metabolites synergistically evoke sensations of
628 muscle fatigue and pain in human subjects. Exp Physiol 99:368-380.
629 Queme F, Taguchi T, Mizumura K, Graven-Nielsen T (2013) Muscular heat and mechanical pain
630 sensitivity after lengthening contractions in humans and animals. J Pain 14:1425-1436.
631 Queme LF, Ross JL, Jankowski MP (2017) Peripheral Mechanisms of Ischemic Myalgia. Front Cell
632 Neurosci 11:419.
633 Queme LF, Ross JL, Lu P, Hudgins RC, Jankowski MP (2016) Dual Modulation of Nociception and
634 Cardiovascular Reflexes during Peripheral Ischemia through P2Y1 Receptor-Dependent
635 Sensitization of Muscle Afferents. Journal of Neuroscience 36:19-30.
636 Queme LF, Weyler AA, Cohen ER, Hudgins RC, Jankowski MP (2020) A dual role for peripheral GDNF
637 signaling in nociception and cardiovascular reflexes in the mouse. Proc Natl Acad Sci U S A
638 117:698-707.
639 Raghavan P, Lu Y, Mirchandani M, Stecco A (2016) Human Recombinant Hyaluronidase Injections For
640 Upper Limb Muscle Stiffness in Individuals With Cerebral Injury: A Case Series. EBioMedicine
641 9:306-313.
642 Raqib R, Ljungdahl A, Lindberg AA, Wretlind B, Andersson U, Andersson J (1996) Dissociation between
643 cytokine mRNA expression and protein production in shigellosis. Eur J Immunol 26:1130-1138.
644 Ross JL, Queme LF, Shank AT, Hudgins RC, Jankowski MP (2014) Sensitization of group III and IV muscle
645 afferents in the mouse after ischemia and reperfusion injury. J Pain 15:1257-1270.
646 Ross JL, Queme LF, Lamb JE, Green KJ, Ford ZK, Jankowski MP (2018) Interleukin 1β inhibition
647 contributes to the antinociceptive effects of voluntary exercise on ischemia/reperfusion-induced
648 hypersensitivity. Pain 159:380-392.
649 Ross JL, Queme LF, Cohen ER, Green KJ, Lu P, Shank AT, An S, Hudgins RC, Jankowski MP (2016) Muscle
650 IL1β Drives Ischemic Myalgia via ASIC3-Mediated Sensory Neuron Sensitization. J Neurosci
651 36:6857-6871.
652 Rüschen H, Aravinth K, Bunce C, Bokre D (2018) Use of hyaluronidase as an adjunct to local anaesthetic
653 eye blocks to reduce intraoperative pain in adults. Cochrane Database Syst Rev 3:Cd010368.
654 Schindler R, Clark BD, Dinarello CA (1990) Dissociation between interleukin-1 beta mRNA and protein
655 synthesis in human peripheral blood mononuclear cells. J Biol Chem 265:10232-10237.
656 Singha NC, Nekoroski T, Zhao C, Symons R, Jiang P, Frost GI, Huang Z, Shepard HM (2015) Tumor-
657 associated hyaluronan limits efficacy of monoclonal antibody therapy. Mol Cancer Ther 14:523-
658 532.
659 Tappe-Theodor A, King T, Morgan MM (2019) Pros and Cons of Clinically Relevant Methods to Assess
660 Pain in Rodents. Neurosci Biobehav Rev 100:335-343.
661 Wynn TA, Vannella KM (2016) Macrophages in Tissue Repair, Regeneration, and Fibrosis. Immunity
662 44:450-462.
663 Yu X, Liu H, Hamel KA, Morvan MG, Yu S, Leff J, Guan Z, Braz JM, Basbaum AI (2020) Dorsal root ganglion
664 macrophages contribute to both the initiation and persistence of neuropathic pain. Nat
665 Commun 11:264.

666

667

668

669

Figure legends:

Figure 1. PEGPH20 decreases voluntary wheel running but does not cause acute mechanical hypersensitivity. A. Voluntary wheel running is significantly decreased up to 3 days after the administration of PEGPH20 (n=12), compared to vehicle controls (n=12). B. Withdrawal thresholds to muscle squeezing are significantly lower 5 days after the administration of PEGPH20 (n=8) compared to vehicle treated mice (n=8). C. There are no significant differences in grip strength between mice treated with PEGPH20 (n=8) vs vehicle treated mice (n=8). Two-way RM ANOVA (Bonferroni post-hoc); A. $F(1,14)=6.654$, $p=0.218$; B. $F(4,56)=5.515$, $p=0.0008$; C. $F(4,56)=0.68$. A-C $*p<0.05$. $**p<0.01$ vs vehicle.

Figure 2. PEGPH20 induces increased response to noxious metabolites in metabo-nociceptive primary muscle afferents. A-D. We did not observe changes in the mechanical thresholds or response patterns of mechanically sensitive neurons after PEGPH20 (n= 18) administration, compared to vehicle controls (n=18). The same can be said of the responses to heat (n=3 per group) or cold (n=4 per group) stimulation. E-F. While there were no changes in the response to chemical stimulation in neurons sensitive to a low concentration of metabolites (Vehicle, n=5; PEGPH20 n=12), injection of PEGPH20 caused a significant increase in the instantaneous frequency of firing in high metabolite responsive neurons (metabo-nociceptors). (Vehicle n=8, PEGPH20 n=9). G. Representative traces of mechanical, thermal, and chemical responses from neurons recorded from either Vehicle or PEGPH20 treated mice. Arrows represent application of stimulus. A-F Mann Whitney U-test, $*p<0.02$ vs vehicle.

692 **Figure 3. PEGPH20 disrupts of skeletal muscle architecture that is accompanied by**
693 **macrophage infiltration.** A. Muscle extracellular membrane (green - WGA) is disrupted 3 days
694 after the administration of PEGPH20. EBD (red) usually remains in intravascular spaces in intact
695 tissue but after hyaluronidase administration it leaks into the affected skeletal muscle. B.
696 Percentage of myofibers positive for EBD 3 days after PEGPH20 administration. C. At the same
697 timepoint macrophages (red - LysM/tdTomato) infiltrate the connective tissue surrounding the
698 skeletal muscle in contrast to the almost non-present macrophages in the vehicle treated animals.
699 White scale bar is 50µm. ***$p<0.001$ χ^2 test.
700
701 **Figure 4. Ablation of macrophages does not prevent decreased voluntary wheel running**
702 **after administration of PEGPH20.** A. Administration of AP for 7 days starting 3 days before
703 PEGPH20 injection removes macrophages from all hindpaw tissues as revealed by the lack of
704 GFP signal (arrows) in the treated animals compared to vehicle treated controls. B.
705 Quantification of GFP signal reveals significantly less signal in AP-treated mice (n=3) vs
706 Vehicle-treated animals (n=3). Ablation of macrophages in MaFIA mice does not prevent the
707 development of decreased voluntary wheel running distance after PEGPH20 (n=12)
708 administration compared to vehicle treated mice (n=12). In fact, the combination of
709 PEGPH20+AP (n=8) used to ablate macrophages prevents the slow recuperation that initiates
710 around 4 days after PEGPH20 administration. B. Total wheel running distance is significantly
711 lower in PEPH20, AP alone (n=8), or PEGPH20+AP treated mice compared to just vehicle
712 treated mice. The total running distance of PEGPH20+AP treated mice was also significantly
713 lower than in animals treated with just PEGPH20 or AP alone. White scale bar is 50 µM B.
714 Unpaired T-test; C. Mixed-effects analysis ($F(2,29) = 19.16$, $p<0.0001$) with Bonferroni post-

715 hoc; D. One-way ANOVA ($F(3,24) = 38.87$, $p<0.001$) with Bonferroni post-hoc. #$p<0.05$,
716 ^$p<0.01$ vs PEGPH20+AP; *$p<0.05$, **$p<0.01$ vs vehicle.
717
718
719
720 **Table 1: General electrophysiological parameters from recordings 1 and 3 days after**
721 **administration of PEGPH20 or Vehicle.** We do not observe any significant differences
722 between electrophysiological recordings performed either 1 or 3 days after treatment in each
723 condition.
724
725 **Table 2: Select DRG gene expression after PEGPH20 administration (1-7 days).** Values
726 indicate % change vs vehicle treated controls. Mean ± SEM. n=4 per group per time point. One-
727 way ANOVA (TrkA $F(4,14)=10.57$, $p=0.0004$; P2X3 $F(4,14)=17.27$, $p<0.0001$; GFRα1
728 $F(4,13)=29.57$, $p<0.0001$; LI1r1 $F(4,12)=8.272$, $p=0.0019$) with Bonferroni post-hoc. * $p<0.05$,
729 ** $p<0.01$, *** $p<0.001$ vs vehicle treated controls. GAPDH CT (mean ± SEM) CTRL: 20.97 ±
730 0.26; D1 19.651 ± 0.07; D3 20.295 ± 0.45 D5 21.2 ± 0.39 D7 22.32 ± 0.82. No significant
731 differences were detected between the CTRL or treatment groups (One-way ANOVA
732 $F(4,14)=3.8$, $p=0.026$).
733
734 **Table 3: Total daily distance traveled after treatment.** Administration of AP alone (n=6)
735 induced changes similar to Vehicle (n=8), PEGPH20 (n=12), and PEGPH20+AP (n=12). The
736 combination of PEGPH20+AP produced significantly lower levels of activity during the first 4
737 days after administration but did not show the recuperation observed by 7 days in both the

738 PEGPH20 or AP alone treated groups. Data from AP alone for day 3 only includes n=2 due to
739 equipment failure that did not allow capture of data for the single time point. 2-way ANOVA,
740 $F(3,34)=12.54$, $p<0.0001$ with Bonferroni post hoc test. *$p<0.05$, **$p<0.01$ vs Vehicle, #$p<0.05$
741 vs PEGPH20.

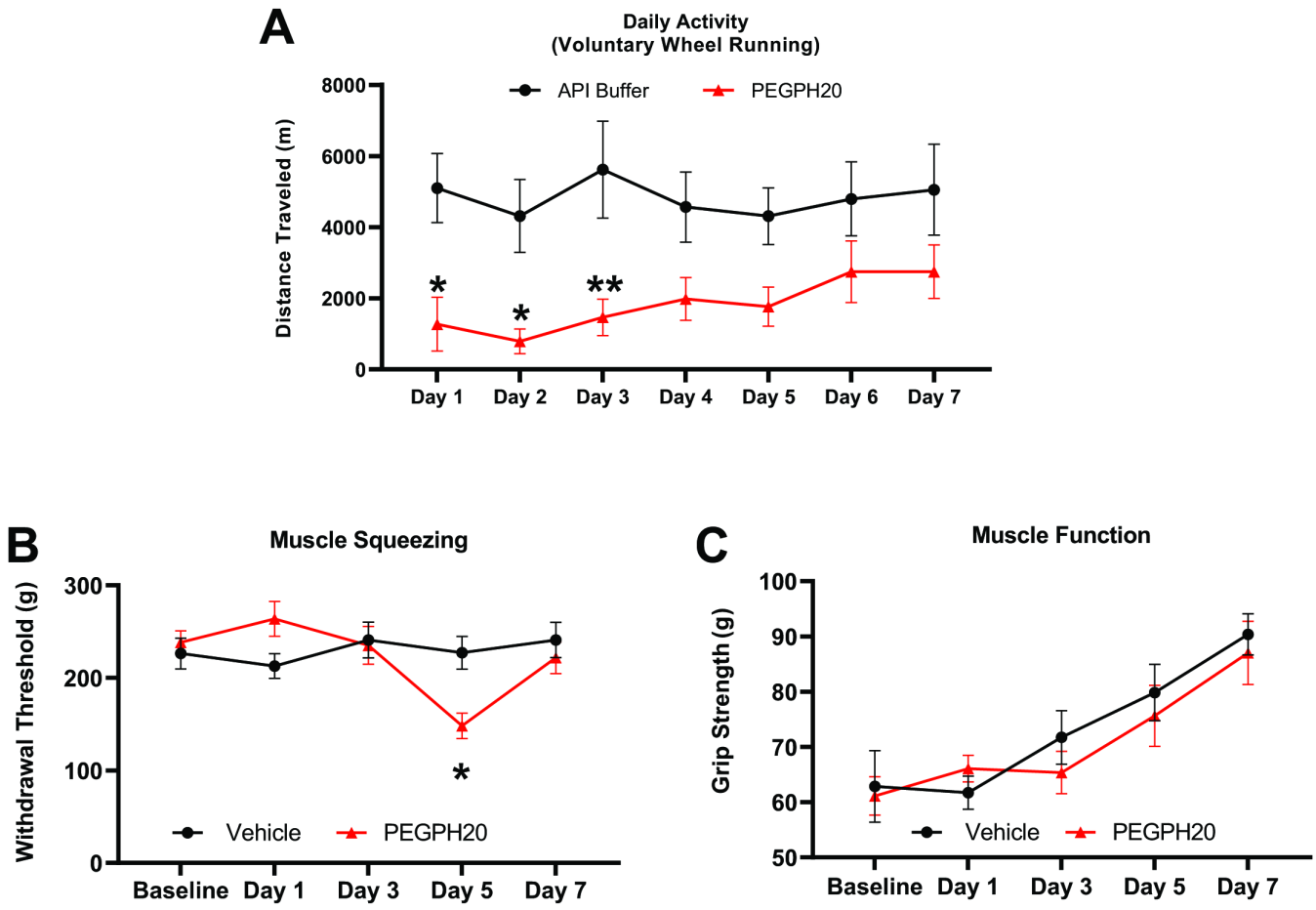

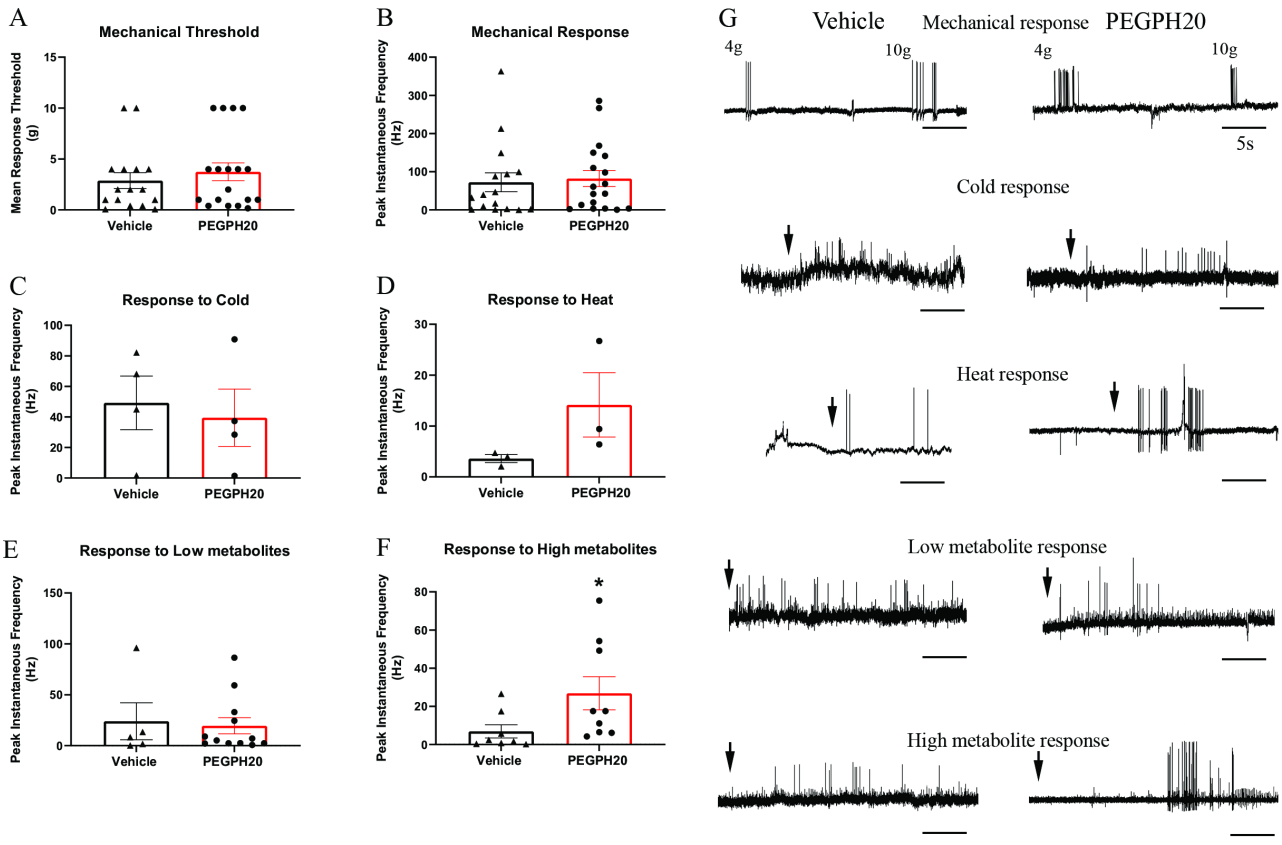

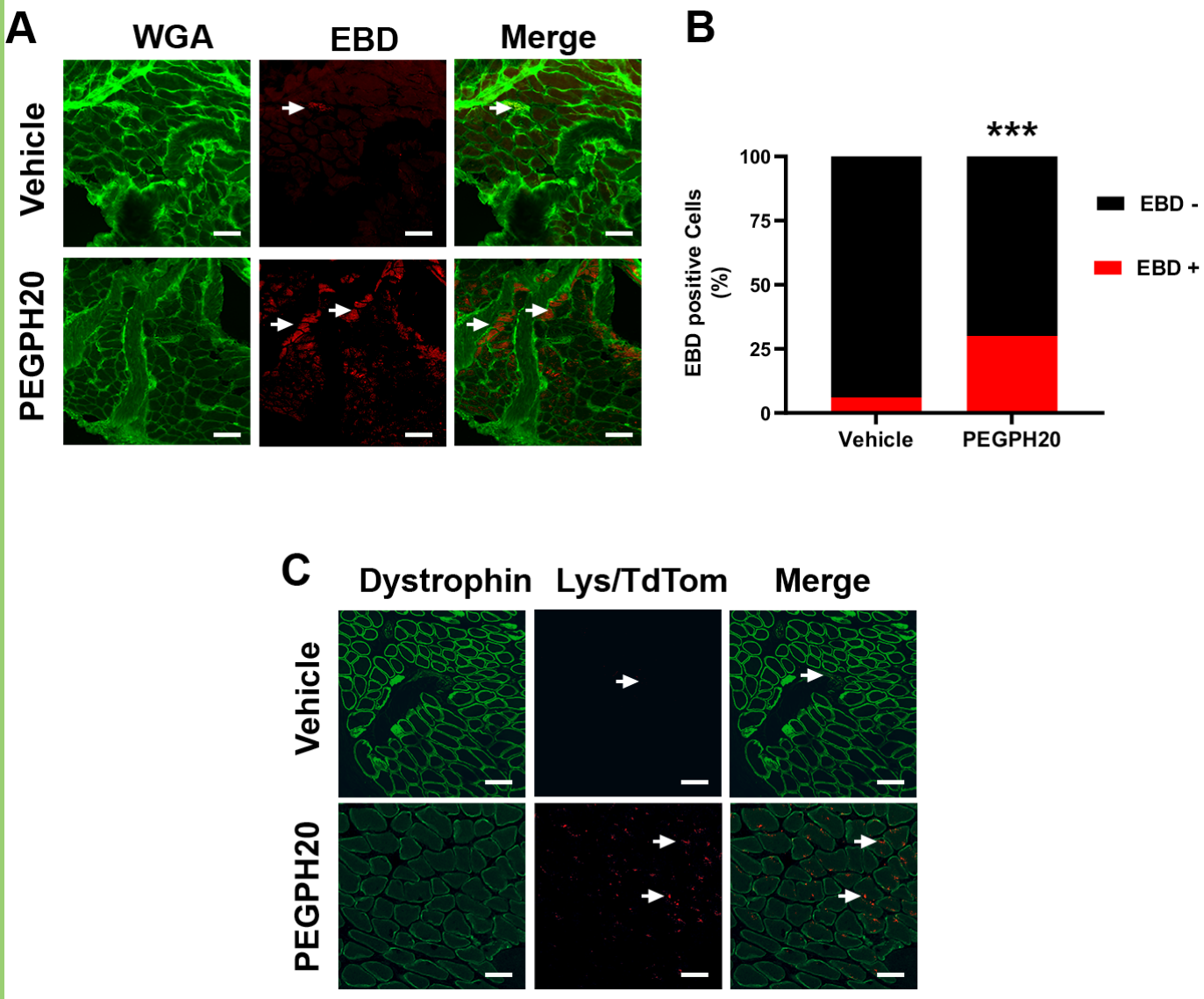

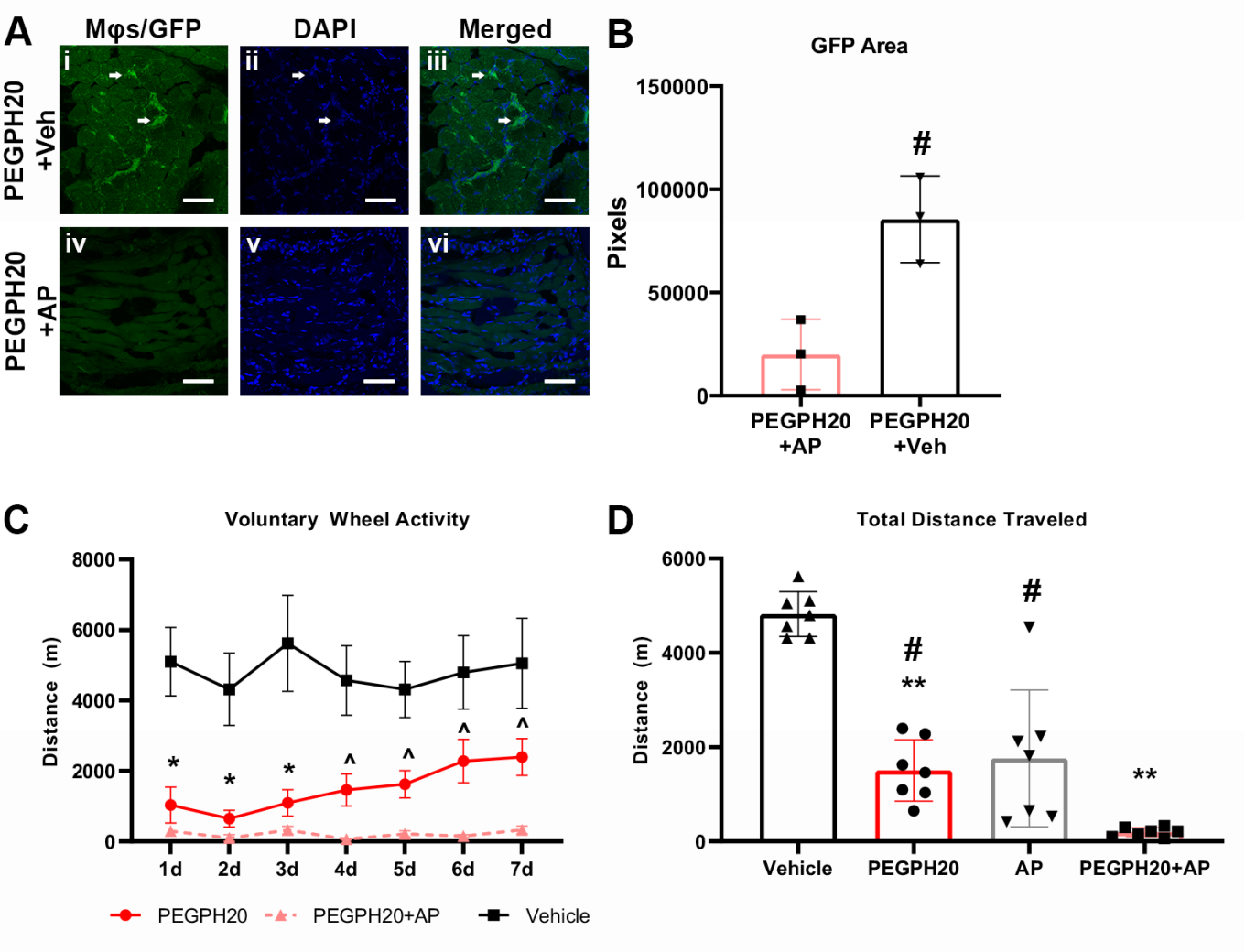

Table 1	Condition	
	Vehicle 1d	**Vehicle 3d**
Conduction Velocity	10.56 ± 1.99 (n=27)	6.71 ± 1.37 (n=21)
Mechanical Threshold	2.77 ± 1.08 (n=9)	4.29 ± 1.52 (n=7)
Mechanical response (Peak IF, Hz)	44.02 ± 18.57 (n=9)	108.80 ± 50.19 (n=7)
Heat response (Peak IF, Hz)	3.03 ± 0.95 (n=2)	4.7 ± 0.0 (n=1)
Cold response (Peak IF, Hz)	63.53 ± 18.53 (n=2)	34.90 ± 33.20 (n=2)
Low Metabolite response (Peak IF, Hz)	13.4 ± 0.0 (n=1)	26.58 ± 23.24 (n=4)
Hight Metabolite response (Peak IF, Hz)	1.39 ± 0.64 (n=3)	8.37 ± 6.19 (n=4)
	Condition	
	PEGPH20 1d	**PEGPH20 3d**
Conduction Velocity	6.487 ± 1.18 (n=24)	10.33 ± 1.92 (n=24)
Mechanical Threshold	5.2 ± 1.11 (n=9)	1.92 ± 1.17 (n=7)
Mechanical response (Peak IF, Hz)	77.41 ± 9.95 (n=9)	88.07 ± 31.53 (n=7)
Heat response (Peak IF, Hz)	26.7 ± 0.0 (n=1)	7.9 ± 1.5 (n=2)
Cold response (Peak IF, Hz)	No cold responses recorded	39.48 ± 18.73 (n=4)
Low Metabolite response (Peak IF, Hz)	3.9 ± 1.45 (n=5)	30.66 ± 12.09 (n=7)
Hight Metabolite response (Peak IF, Hz)	13.16 ± 4.62 (n=4)	37.82 ± 14.05 (n=5)

Table 2

Gene	D1	D3	D5	D7
TrkA	21.9 ± 13.5	70.2 ± 8.0	-60.7 ± 13.4*	-52.2 ±30.3
P2X3	49.8 ± 13.1	458.3 ± 13.8***	114.8 ± 29.2	459.6 ± 25.9**
P2X5	-4.4 ± 10.2	-63.9 ± 39.1	-37.0 ± 38.9	-62.8 ± 15.9
TRPV1	9.3 ± 15.2	58.6 ± 9.0	-66.3 ± 20.1	-63.4 ± 49.4
TRPA1	-23.8 ± 12.6	-13.66 ± 113.03	58.3 ± 28.6	-32.99 ± 37.53
ASIC3	0.8 ± 7.2	7.5 ± 5.0	-82.77 ± 110.1	-76.33 ± 61.62
GFRα1	-2.8 ± 7.3	-81.8 ± 12.1**	-93.1 ± 26.8***	-97.6 ± 56.1***
GFRα2	30.3 ± 18.8	-44.8 ± 95.9	-55.9 ± 41.4	-69.2 ± 29.4
GFRα3	-7.6 ± 5.5	-60.5 ± 120.6	-18.5 ± 37.31	-37.8± 14.72
IL1r1	-17.9 ± 11.9	-90.1 ± 85.3*	-83.3 ± 28.5	-89.1± 7.9*

Table 3	Vehicle	PEGPH20	PEGPH20+AP	AP
1d	5100.08 ± 972.65 m	1034.07 ± 507.76 m*	297.27 ± 63.98 m**	2118.52 ± 622.81 m
2d	4314.84 ± 1028.88 m	647.95 ± 237.69 m*	97.19 ± 92.70 m*	529.68 ± 225.32 m*
3d	5617.62 ± 1360.53 m	1091.83 ± 372.54 m	319.24 ± 113.41 m*	4541.73 ± 2236.27 m
4d	4566.33 ± 987.13 m	1457.09 ± 454.28 m*	64.62 ± 22.11 m*	419.32 ± 340.40 m*
5d	4308.31 ± 793.60 m	1624.41 ± 386.50 m*	216.20 ± 85.72 m** $^{\#}$	1819.74 ± 1368.44 m*
6d	4795.18 ± 1037.20 m	2278.82 ± 616.13 m	151.05 ± 40.59 m* $^{\#}$	646.48 ± 496.81 m*
7d	5052.14 ± 1275.32 m	2393.98 ± 522.54 m	329.55 ± 108.71 m* $^{\#}$	2223.02 ± 1497.26 m